

Wearable Biosupercapacitor: Harvesting and Storing Energy from Sweat

Jian Lv, Lu Yin, Xiaohong Chen, Itthipon Jeerapan, Cristian A. Silva, Yang Li, Minh Le, Zhihua Lin, Luwen Wang, Alexander Trifonov, Sheng Xu, Serge Cosnier,* and Joseph Wang*

This work demonstrates the first example of sweat-based wearable and stretchable biosupercapacitors (BSCs), capable of generating high-power pulses from human activity. The all-printed, dual-functional, conformal BSC platform can harvest and store energy from sweat lactate. By integrating energy harvesting and storage functionalities on the same footprint of a single epidermal device, the new wearable energy system can deliver high-power pulses and be rapidly self-charged by bioenergy conversion of sweat lactate generated from human activity while simplifying the design and fabrication. The mechanical robustness and conformability of the device are realized through island-bridge patterns and strain-enduring inks. The enhanced capacitance of the BSC is realized by the synergistic effect of carbon nanotube ink with electrodeposited polypyrrole on the anode and of porous cauliflower-like platinum on the cathode. In the presence of lactate, the BSC shows high power in pulsed output and stable cycling performance. Furthermore, the wearable device can store energy and deliver high-power pulses long after the perspiration stopped. The self-charging hybrid wearable device obtained high power of 1.7 mW cm^{-2} *in vitro*, and $343 \text{ } \mu\text{W cm}^{-2}$ on the body during exercise, suggesting considerable potential as a power source for the next generation of wearable electronics.

and stretchable electronics, ranging from mechanical and electrochemical sensors^[3–5] to complex systems such as multi-sensor arrays, transistor arrays, or electronic displays,^[6–9] have been assembled into a comprehensive ecosystem of various class of devices with distinct functionalities. However, one of the main challenges that impede such wide adoption of flexible and stretchable wearable electronics is the lack of an equally flexible, stretchable, and miniaturized energy source that can supply sufficient power over extended periods. Depending on the functionalities of the device,^[10] most wearable electronics consume power ranging from as low as nano-watts to more common milli-watts, with expected usage ranging from a few hours to multiple days. Tremendous efforts have been dedicated to the fabrication of wearable systems to harvest and store energy from various sources, such as human movement, perspiration, sunlight, or the air.^[11–15] Among these, wearable biofuel cells (BFCs) that

convert chemical energy from human perspiration to electrical energy via enzymatic electrochemical reactions are considered a promising potential solution.^[16–20] Nevertheless, one of the key shortcomings of such sweat-based energy harvesters is the need for the constant supply of fuel from human perspiration and the presence of the oxidizer. To address this issue, hybrid devices that combine energy harvesting and storage modules have been reported.^[21,22] For example, we demonstrated previously a stretchable textile-based wearable hybrid BFC-supercapacitor (SC) device, where energy is generated from human sweat by the BFC and stored in the SC for later use.^[21] However, these integrated hybrid devices still rely on the external connection of the two separate harvesting and storage modules. Some recent efforts demonstrated the possibility of endowing multiple functionalities onto one single device via material innovations, storing energy in multiple modes, or simultaneously harvesting and storing mechanical and chemical energy; however, such multi-functional materials and designs have not been demonstrated for wearable sweat-based energy systems.^[23–25] We envision the integration of harvesting and energy storage functionalities at the material level would be more beneficial for

1. Introduction

In recent years, the field of wearable electronics has been experiencing a transition from rigid, bulky, and non-conformal devices to miniaturized, flexible, and stretchable devices that conform and adapt to the human body with high intimacy.^[1,2] Built upon the work of numerous researchers, the state-of-the-art flexible

Dr. J. Lv, L. Yin, Dr. X. Chen, Dr. I. Jeerapan, C. A. Silva, Y. Li, M. Le, Dr. Z. Lin, Dr. L. Wang, Dr. A. Trifonov, Prof. S. Xu, Prof. J. Wang
Department of NanoEngineering
University of California San Diego
La Jolla, CA 92093, USA
E-mail: josephwang@ucsd.edu
Dr. X. Chen, Prof. S. Cosnier
Université Grenoble Alpes-CNRS
DCM, UMR 5250, Grenoble F-38000, France
E-mail: Serge.Cosnier@univ-grenoble-alpes.fr

 The ORCID identification number(s) for the author(s) of this article can be found under <https://doi.org/10.1002/adfm.202102915>.

DOI: 10.1002/adfm.202102915

the miniaturization of a sustainable high-power energy supply unit for wearable electronics.

Self-charging biosupercapacitors (BSCs) that can store energy and be self-charged via chemical or solar energy conversion have recently attracted considerable attention.^[26–28] BSCs are biomaterial-based two-electrode systems that combine both BFC and SC functionalities in a single device.^[29] Compared with traditional BFCs, the BSCs can generate higher power pulses due to their high-capacitance electrodes that allow rapid discharges. Supercapacitance can be realized by using nanostructured electrode materials to increase electrochemical double-layer capacitance^[25] or by the addition of redox molecules^[30] and conductive polymers^[31] to endow pseudocapacitive behavior. Compared with traditional SCs, which require external power input, self-charging BSCs rely on biocatalysts, such as microbes, organelles, or enzymes, immobilized onto highly capacitive material that allows energy conversion from body fluids or sunlight and its subsequent storage.^[29] The dual-functionality feature of BSCs can greatly simplify the design of wearable systems as no external connection is needed, hence improving the energy efficiency and facilitating the miniaturization of the electronic device. For chemical-energy-based BSCs, glucose- and other fuel-based BSCs have been studied.^[27] However, to the best of our knowledge, there are no reports on sweat-operated BSCs for on-body wearable applications. For a wearable BSC, the flexibility, stretchability, and skin conformity of the device are of considerable importance. Different materials have been used previously to fabricate electrodes for BSCs, including carbon paper, carbon nanotube (CNT) pellets, or graphite foil.^[17,25,30,31] However, these materials are either bulky, rigid, or fragile, and therefore cannot serve as suitable candidates for stretchable conformal wearable electronic devices.

In this work, we demonstrate the first example of an all-printed dual-functional stretchable and wearable BSC, fabricated on top of low-elastic modulus and adhesive elastic films, to harvest and store energy from sweat while maintaining intimate contact with the human skin. This wearable hybrid device, functioning as both a BFC and an SC, is demonstrated to deliver high-power pulses and be rapidly self-recharged using enzymatic oxidation of lactate biofuel from human perspiration. Compared to an early multi-module BFC and SC system,^[21] this work enabled material-level integration of both functionalities on the same set of electrodes, thus reducing the system complexity and minimizing the device footprint. A scalable and low-cost screen-printing process, using stress-enduring inks, is used to fabricate the BSC (combining the BFC and SC functions on the same printed anode and cathode) and meeting the softness, stretchability, and scalability requirements for this skin-worn wearable device. The stable, conformal, and stretchable energy harvesting-storage dual-function device has been realized through the highly efficient planar electrode design with an “island-bridge” structure and the use of such strain-enduring inks.^[2,32] The island-bridge structure is fabricated on a soft silicone rubber substrate; a non-elastic backbone layer is printed at the bottom of the active electrode “islands” for mechanical support, while silver interconnections are printed in serpentine patterns as “bridges.”^[33] The stress in the electrode area is thereby distributed to the surrounding flexible region when the device is under deformation, hence ensuring

attractive mechanical resiliency. Compared to the common lactate/O₂ BFC, the greatly enhanced capacitance of the BSC is achieved by the synergistic effect of the CNT-based ink and the electrodeposited polypyrrole (PPy) conductive polymer on the anode and of the high-surface-area cauliflower-like structured porous Pt on the cathode. The resulting wearable dual-functional BSC can support high-power pulsed output while maintaining stable charge–discharge performance in human sweat-level lactate. The self-rechargeable hybrid device demonstrated harvesting high power up to 1.7 mW cm^{−2} and can be mounted on user’s arm for energy harvesting, suggesting its considerable potential as a power source for the next generation of wearable devices.

2. Results and Discussion

The new soft, dual functional, and skin-worn BSC, integrated on a conformal elastomeric substrate, was designed in a planar structure to harvest and store energy from human sweat (Figure 1A,B). The surface and structure of the device have been tailored to merge the BFC and SC functions into one single wearable device (Figure 1C). The surface of both electrodes was thus modified to combine the energy harvesting capability with the energy storage functionality. PPy is an attractive electrode material for SC operation owing to its favorable conductivity and pseudocapacitance.^[34,35] Therefore, the anode was assembled based on the PPy-electrodeposited multiwalled CNTs and decorated by lactate oxidase (LOx) enzyme, mediated by 1,4-naphthoquinone (NQ) relay units. On the anode, the LOx-catalyzed lactate oxidation is facilitated by the NQ that regenerates the flavine mononucleotide cofactor, allowing continuous fuel oxidation. The cathode is composed of the same CNTs-based electrode, functionalized by an electrodeposited high-surface-area porous Pt catalytic layer, offering high electrochemical double-layer capacitance. The Pt-catalyzed oxygen reduction reaction (ORR) provides a driving force for the continuous electron flow from the anode to the cathode, producing and storing electric energy on the same device.

A phosphate buffer solution–polyvinyl alcohol (PBS–PVA) hydrogel was implemented as the electrolyte that allowed free diffusion of sweat to the electrode surface.^[22] By such design, the wearable BSC can be continuously charged in open circuit mode, then generating stable high-power pulses on the order of seconds when discharged at a high current (Figure 1D–F).

Screen printing, a low-cost and large-scale fabrication method, was used to manufacture the stretchable and conformal BSC device (Figure S1, Supporting Information). The design of the device included an “island-bridge” configuration and was fabricated with customized strain-enduring inks. The “island-bridge” structure is designed to maximize the mechanical robustness of the device, where the functional electrodes are separated into several individual compartments as “islands” and are interconnected by highly stretchable conductive silver interconnections, which act as the “bridges.” Besides, a flexible, non-stretchable “skeleton” layer with high elastic modulus and mechanical strength is added below the “islands” as reinforcement to further minimize any strain applied to the electrodes.^[33] As a result, the strain induced by external deformation can be

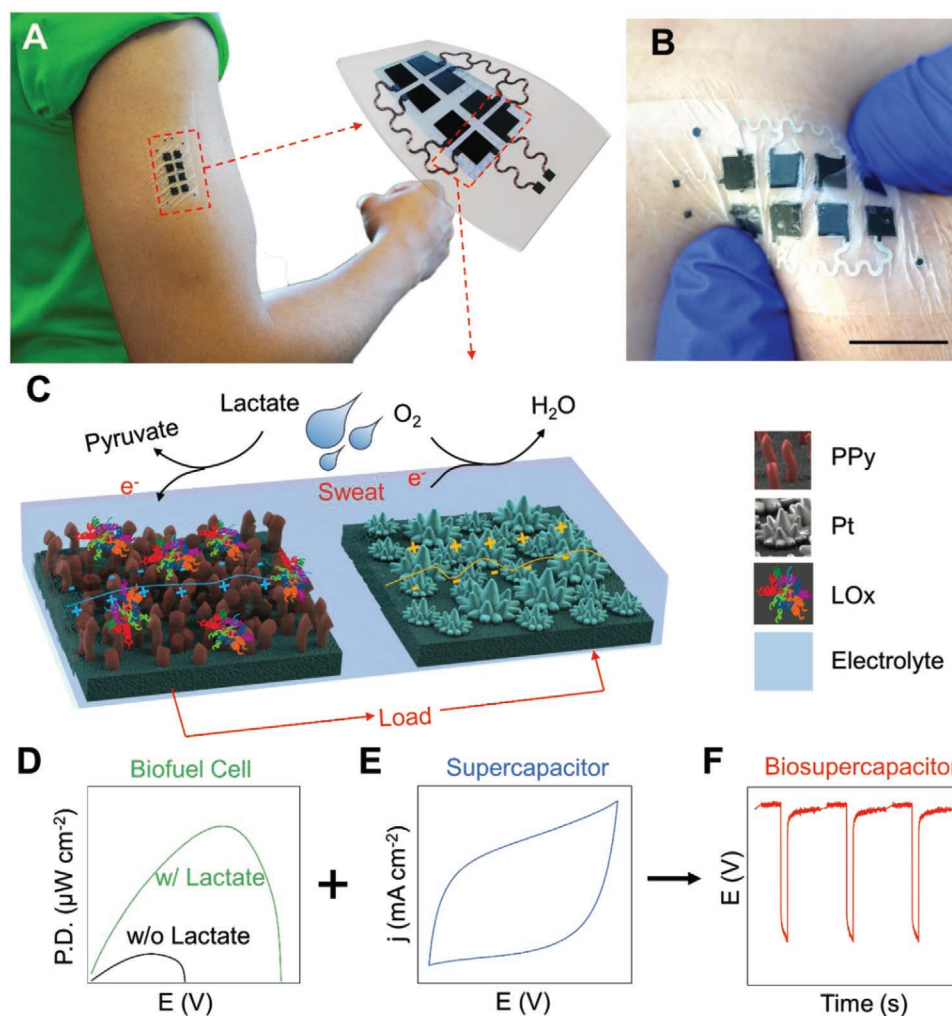


Figure 1. Schematic illustration of the epidermal BSC patch. A) Schematic illustration of the skin-mountable dual-functional (energy harvesting and energy storage) BSC device. B) Photograph of the stretchable, dual-functional BSC device on human skin, scale bar: 2 cm. C) Schematics of the redox energy generation and capacitive energy storage from sweat lactate by the single device. D–F) Key characteristics of the BSC combining a BFC (D) and SC (E) to form a dual-functional self-charging BSC that supports high-power pulse discharge (F).

effectively dispersed around the electrode “islands,” and any adverse effects yielded from the deformation can be minimized. Adopted from our previous work, the CNTs and silver inks used in the printing of the stretchable electrodes were customized to obtain outstanding flexibility and stretchability.^[36] The stretchability of the CNT ink is inherited from its elastic polyurethane (PU) binder, while the highly conductive and flexible silver ink is made of silver flakes and an elastomeric copolymer binder (polystyrene-block-polyisoprene-block-polystyrene; SIS).^[21,36] Working in conjunction, the elaborate “island-bridge” structure design and ink formulation endow the printed electrodes with electrical conductivity and stability during mechanical deformation.

The morphology of the electrode surfaces was investigated by scanning electron microscopy (SEM). Compared with the unmodified CNT electrode (Figure 2A), the modification of the anode and the cathode has visibly improved the porosity and tortuosity of electrodes (Figure 2B,C, respectively). The apparent improvement in surface roughness is expected to

contribute to enhancing the capacitive behavior of the modified BFC-based BSC. The deposited Pt and PPy were verified by the SEM imaging with energy-dispersive X-ray spectroscopy (EDS) shown in Figure S2, Supporting Information. The cathode and anode were characterized by linear and cyclic voltammeteries, demonstrated in Figures S3,S4, Supporting Information, supporting the essential role of porous Pt and LOx as catalysts for oxygen reduction and lactate oxidation, with a catalytic onset potential of $E \approx 0.33$ and -0.15 V versus Ag/AgCl, respectively, and improved the electrode’s capacitance. The choice of the PPy, as a capacitive polymer, imparts a porous electrode morphology with increased surface area and pseudocapacitance along with an overall stable positive charge in the range of 4–8 pH, which is within the range of the pH of human perspiration.^[37] The protonation/deprotonation of nitrogen atoms of the polymer is a primary reason for pseudocapacitive behavior and the ability to store the charge. Evidently, on the bioanode, a deposited porous PPy film has allowed stable LOx immobilization on the carbonaceous electrode matrix and significantly improved the

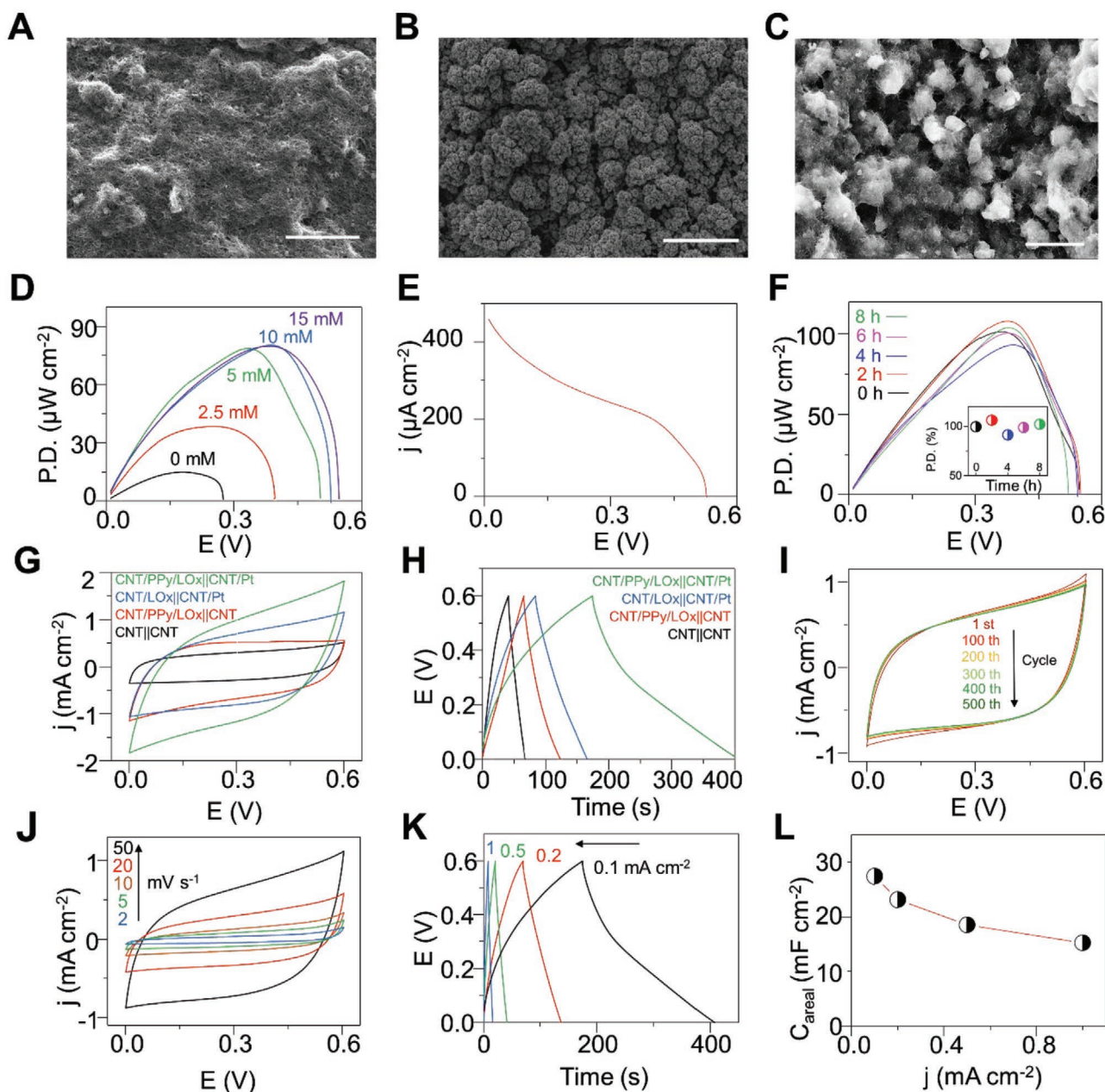


Figure 2. BSC bioelectrocatalytic and capacitive behavior characterizations. SEM images of A) printed pristine CNT electrode, B) CNT electrode with electrodeposited Pt as the catalyst, and C) CNT electrode with electrodeposited PPy. Scale bar: (A,B) 10 μm ; (C) 5 μm . D) The power density versus voltage plots of the stretchable BSC using different lactate concentrations (0, 2.5, 5, 10, and 15 mM) in 0.5 M PBS (pH 7.4). E) Polarization curve of the BSC in the presence of 10 mM lactate. F) Long-term stability of the BSC in the presence of 10 mM lactate over 8 h. Inset: power density at 0.38 V over this period. BSC capacitive behavior study: G) CV (scan rate: 100 mV s^{-1}) and H) galvanostatic charge–discharge curves (current density: 0.1 mA cm^{-1}) of the BSC in 2-electrode system with different levels of functionalization; I) the stability of the BSC is tested with 500 CV cycles at the scan rate of 50 mV s^{-1} ; J) CV curves of the fully functionalized BSC at different scan rates; K) GCD curves of the BSC at different charge–discharge current densities (0.1, 0.2, 0.5, and 1.0 mA cm^{-2}) and L) the corresponding areal capacitance.

electrode's capacitance (by approximately twofolds; Figure S5, Supporting Information).

The energy harvesting performance of the BSC, consisting of the LOx/NQ/PPy-based bioanode and the porous Pt-based cathode, was characterized. Figure 2D shows the power density of BFC when discharged against variable resistances in the presence of different lactate levels. The data plots indicate

a typical power curve behavior, showing an increase in open-circuit voltage (OCV) from $E = 0.28$ to 0.55 V upon elevating the lactate concentration from 0 to 15 mM. The power values were also enhanced upon increasing the lactate level until reaching saturation at 10 mM lactate, with a maximal power density of 80 $\mu\text{W cm}^{-2}$ at $E = 0.38$ V. Over the range of 0–5 mM lactate, the power increases linearly with the fuel concentration,

demonstrating an increase of $\approx 9 \mu\text{W cm}^{-2} \text{ mm}^{-1}$. A maximum OCV of $E = 0.55 \text{ V}$ and the closed-circuit current density of $460 \mu\text{A cm}^{-2}$ were reached at 10 mM lactate (Figure 2E). Furthermore, a long-term stability test of the BSC, shown in Figure 2F, demonstrates a stable output with a small standard deviation of 6.4% during the 8 h study period, and effective output of around $100 \mu\text{W cm}^{-2}$ at 0.38 V . It should be noted that the OCV established by the cell exceeds the theoretical value of 0.48 V calculated based on electrochemical characterization of the LOx anode and Pt cathode (Figures S3, S4, Supporting Information). This effect is attributed to the presence of the redox-active PPy with a charge-storing pseudocapacitance.^[38] As the charging of the BSC device increases significantly at higher voltages, the OCV of 0.55 V , established within 2 h, was considered as a practical OCV value.

The capacitance of the BSC can be maximized through several strategies. A CNT-based composite ink was chosen for its attractive active surface area, which greatly enhances the double-layer capacitance of the electrodes, based on our early studies.^[21,39] PPy is electropolymerized onto the anode from a pyrrole-containing KClO_4 solution to endow higher capacitance to the bioanode. Pt is electroplated onto the cathode at $E = -0.95 \text{ V}$ versus Ag/AgCl to facilitate ORR. Such deposition results in a cauliflower-like structured, high-surface-area Pt, which further enhances the double-layer capacitance of the BSC. Cyclic voltammetry (CV), used for characterization, demonstrates the significant improvement in BSC capacitance after the PPy and Pt functionalization of the anodes and cathodes, respectively (Figure 2G). LOx is thereafter drop-cast onto the anode and immobilized with chitosan. The effect of the capacitive behavior of the BSC was further validated via the galvanostatic charge–discharge (GCD) technique with different current densities. In Figure 2H, GCD is conducted between 0 and 0.6 V , and the samples with and without PPy and Pt functionalization were tested at a discharge rate of 0.1 mA cm^{-2} to confirm the increase in capacitance of such treatments. Differences of a two-, three-, and a nearly fivefold increase in capacitance were observed after the functionalization of Pt alone, PPy alone, and of both Pt and PPy, respectively. The immobilization of LOx leads to a slight decrease in capacitance, demonstrated via electrochemical impedance spectroscopy and GCD method (Figures S6, S7, Supporting Information, respectively) due to partial insulation caused by the enzymatic protein shell and the use of chitosan, which reduces the active surface area and increases the interfacial charge transfer resistance of the electrode. Aiming to test the cyclability of the BSC, 500 CV cycles were performed at a scan rate of 50 mV s^{-1} . The results, displayed in Figure 2I, indicate only a minor capacitance loss of 4% over time. Figure 2J displays cyclic voltammograms of the BSC at scan rates of $5\text{--}50 \text{ mV s}^{-1}$. A rectangular-shaped response, with slight polarization, is observed, indicating the highly capacitive behavior associated with the high surface area and PPy functionalization. In addition, symmetrical charge–discharge behavior was observed across all the current densities used in GCD, Figure 2K. The capacitance of the BSC decreases upon increasing the current density from 0.1 to 1.0 mA cm^{-2} , as shown in Figure 2L. The obtained highest areal capacitance and areal power density of the BSC were calculated to be 27.2 mF cm^{-2} and 0.22 mW cm^{-2} , respectively ($\approx 2.4 \text{ F g}^{-1}$ and

$\approx 20 \text{ mW g}^{-1}$ for the sum of active electrode material weighed $\approx 11 \text{ mg cm}^{-2}$), which are considered very advantageous compared to reported BSC literature as shown in Table S1, Supporting Information. To determine the self-discharge rate of the BSC, its electrical potential was continuously monitored in the absence of lactate, demonstrating the ability to maintain a voltage above 0.4 V for over 100 min after charging to 0.55 V (Figure S8, Supporting Information).

The ability of the dual-functional BSC to deliver high-power pulses was evaluated using current-pulse chronopotentiometry (CP). The BSC was discharged at 1 mA cm^{-2} for 10 ms and left to recharge for 1 min in the absence and presence of 10 mM lactate. The results shown in Figure 3A indicate that in the absence of fuel, the OCV of the BSC is only 0.16 V and a small power density of 0.13 mW cm^{-2} is delivered. In contrast, in the presence of 10 mM lactate, the OCV and pulse power increase to 0.55 V and 0.5 mW cm^{-2} , respectively, indicating the indispensable role of lactate for self-charging BSC.

The performance of the hybrid device was evaluated by applying different current density 10 ms-pulses, ranging from 1 to 10 mA cm^{-2} . As shown in Figure 3B, after applying the short current pulses, the BSC can deliver power using the charges stored in the device and then quickly recover to its initial potential value due to the continuous biocatalytic conversion of lactate and O_2 in the biofuel system. The overlay of the potential drop peak is displayed in Figure 3C, where a fast ohmic drop and a subsequent slower voltage drop due to capacitance discharge can be observed. These results demonstrate the ability of BSC to withstand a high current density discharge, reaching up to 10 mA cm^{-2} . The plot of the calculated power density versus discharge current density, shown in Figure 3D, indicates a maximum power density of 1.7 mW cm^{-2} at 75 mA cm^{-2} . The detailed method of power density calculation is presented in Figure S9, Supporting Information. These values are 20 times higher than the power delivered by BFC in continuous discharge mode. Such a high power density indicates the great potential of the BSC to power medical devices, such as insulin pumps or wearable electronic devices, for example, wireless transmitters.^[40]

To evaluate the long-time operational stability of the device, a $10 \text{ ms } 1 \text{ mA cm}^{-2}$ current pulses were applied every 30 s for 1 h; the potential evolution is presented in Figure 3E. The BSC can maintain a stable voltage drop and quickly recovers to its initial voltage after each current pulse over the long-time operation. The calculated relative pulse power density is shown in the inset of Figure 3E, where no significant performance decrease is observed over 120 cycles. Extended pulsed discharge over 12 h is demonstrated in Figure S10, Supporting Information, which shows only minor fluctuations in power and capacitance among thousands of cycles. The performance of the BSC was also evaluated by applying a constant discharge current (0.1 mA cm^{-2}), as shown in Figure 3F. Without lactate, the device cannot sustain the discharge and was not able to recharge to OCV above 0.3 V , whereas in the presence of lactate, the BSC can sustain constant discharge for $\approx 30 \text{ min}$ and can be self-charged to the original voltage, dictated by the fuel concentration. It is worth noting that in contrast to the results demonstrated in Figure 2K, the addition of the 10 mM lactate was able to significantly extend the discharge time due to the bioelectrocatalytic reactions that simultaneously charge the BSC.

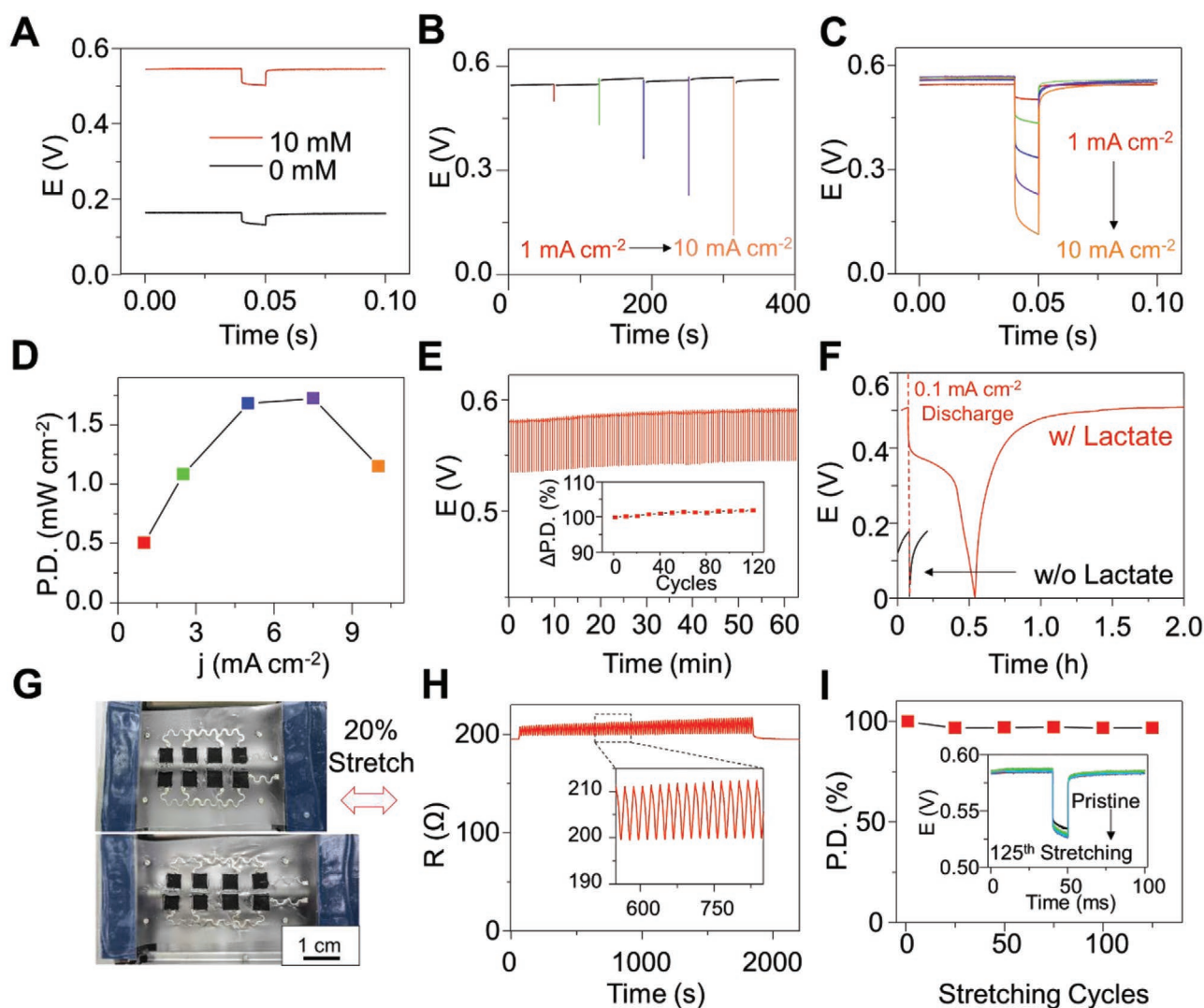


Figure 3. BSC self-charge and pulsed discharge behavior characterizations. A) Potential profile of BSC discharge at 1 mA cm^{-2} current pulse in 0 and 10 mM lactate. B) Potential profile of BSC discharge at 1, 2.5, 5, 7.5, and 10 mA cm^{-2} over 10 ms. C) Overlay of the BSC potential peak profile and D) the calculated power density at different discharge current densities. E) The stability of potential profile of BSC discharge at 1 mA cm^{-2} during 1 h with a 30 s resting time. F) The discharge–self-charge curve of BSC with and without the presence of 10 mM lactate. G) Image of the wearable BSC under 20% stretching. scale bar: 1 cm. H) Resistance profile during stretching, (inset) zoom of resistance fluctuations. I) The stability of the power density profile of BSC discharge at 1 mA cm^{-2} for 125 stretching cycles and (inset) discharge–self-charging curves.

To highlight the flexibility and stretchability of this wearable self-charging BSC, its mechanical resiliency toward external strain was tested by implementing resistance and CP tests on the SCs before and after stretching. The resistance measurement during continuous stretching is demonstrated in Figure 3G and Video S1, Supporting Information. The resistance profile during measuring is shown in Figure 3H, where the resistance is fluctuating around 205Ω with a 5% deviation that corresponds to the continuous deformation of the electrode during measurement to adjust to the external strain. The exceptional mechanical stability allows the resistance to recover to its original value after numerous mechanical deformations. The electrochemical behavior of the anodes and cathodes was measured before and after 100 cycles of 180° bending (3 mm diameter, inward and outward) and 20% stretching

(along lengthwise) via CV (Figure S11, Supporting Information), while monitoring their morphological changes via SEM (Figure S12, Supporting Information). The results indicate minimal mechanical damage and changes in performance. Figure 3I shows the stability of the potential profile of BSC discharged at 1 mA cm^{-2} for 125 stretching cycles. A 10 ms current pulse was applied after every 25 cycles. The power was maintained at over 96% of the maximal value after 125 cycles of 20% stretching. The results demonstrate the robustness of the hybrid device, confirming its potential as a power source for on-body applications.

To demonstrate the wearable BSC in real-life scenarios, the printed device was mounted on the arm of a volunteer during the stationary cycling exercise (Figure 4A). The whole process consists of three periods: a) mounting the BSC and start cycling,

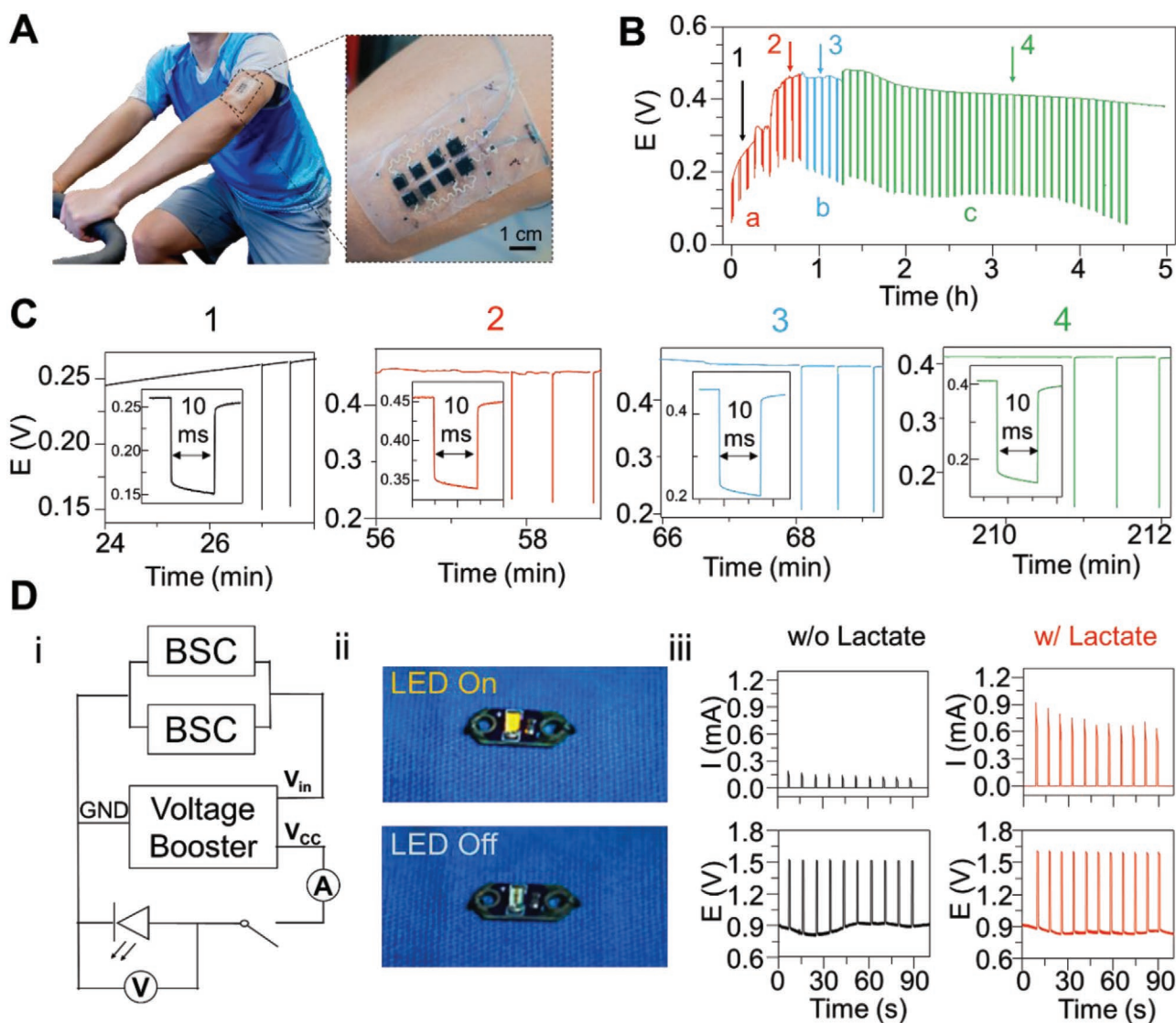


Figure 4. BSC On-body behavior. A) The printed wearable BSC was mounted on the arm of a subject. B) The voltage monitoring of the wearable BSC: a) during the on-body constant cycling exercise, b) after cycling exercise, and c) unloading the BSC from the skin. C) The pulse outputs of the wearable BSC 1) during cycling exercise, 2) when the voltage output reaches a stable state, 3) after the exercise, and 4) after removing the wearable BSC from the skin for 2 h. D) i) Circuit schematics demonstrate using two BSC patches to power an LED via a voltage booster. ii) Photograph of the LED during and after the pulsed discharge. iii) The pulsed discharge profile of the BSCs in the absence and presence of 10 mM lactate.

b) stop cycling, and c) removing the wearable BSC from the arm of the volunteer. Three pulses with the 1 mA cm^{-2} current were performed every 5 min, and the voltage of the device was recorded (Figure 4B). The OCV of the BSC was around 0.17 V before the sweating and reached 0.48 V after 60 min of cycling. The OCV dropped to around 0.46 V when the volunteer stopped cycling. After 25 min of resting, the printed BSC was removed from the volunteer's arm. The OCV was observed to rapidly regenerate to 0.48 V due to exposure of the device to additional oxygen, enhancing the reduction reaction on the Pt cathode. Even after removing the BSC from the volunteer's arm for 230 min, the OCV of the BSC was still retained at 0.38 V. The pulse output operated at 1 mA cm^{-2} current for 10 ms during these different periods is shown in Figure 4C. The power density of the wearable BSC increased from $151 \mu\text{W cm}^{-2}$ (Point 1)

to $343 \mu\text{W cm}^{-2}$ (Point 2), then decreased to $208 \mu\text{W cm}^{-2}$ when the volunteer stopped exercising (Point 3) and decreased gradually upon removing the BSC from the skin (Point 4). The power density of the pulses in the whole testing process is shown in Figure S13, Supporting Information, demonstrating that the power of the device peaks with the exercise and drops steadily to $\approx 150 \mu\text{W cm}^{-2}$ after the exercise stopped. Such performance persisted even after the patch was removed from the body, as the residual stored energy continued to be discharged for another 4 h.

The capability of the BSC to empower commercial electronics is demonstrated in Figure 4D (i) using a simple assembled circuit. Two BSC patches are thus connected in parallel, and the output voltage is boosted via a DC–DC voltage booster. The photo image of a flexible DC–DC voltage

booster with laser-cut copper wiring is shown in Figure S14, Supporting Information. The output signal from the booster was connected to an LED and was controlled by a switch. To visualize the operation of BSCs, they were connected to an LED for 1 s every 10 s, which allow the BSCs to discharge in a pulse then self-recharge (Figure 4D (ii)). The discharge and self-charge current and voltage profiles are demonstrated in Figure 4D (iii), a small current drop is observed during the 1 s discharge. Near the turn-on voltage of ≈ 1.6 V for the LED, the presence of the lactate allows high current discharge, illuminating the LED in bursts, whereas the absence of lactate cannot provide enough current to surpass the turn-on voltage of the LED. A larger current drop is observed in the 5-min extended discharge, as shown in Figure S15, Supporting Information. The advantage that the pulsed discharge of the BSC exhibits in such use case involves a high-power pulsed discharge that can sustain the short-term power draw and quickly recovers, whereas the current drops exponentially after the extended discharge, which takes a longer period to recover afterward.

3. Conclusion

In this work, we demonstrated the first example of an all-printed, stretchable dual-functional BSC for harvesting and storing energy from metabolic sweat lactate. This hybrid device can rapidly self-charge from autonomous lactate/ O_2 redox reactions and deliver high-power pulses due to its simultaneous function as both a BFC and a SC. A scalable and low-cost screen-printing technique has been used to fabricate the wearable device, merging these BFC and SC functions on a single footprint. The device was fabricated on top of low-elastic modulus adhesive elastic films for maintaining intimate contact with human skin during rigorous exercises. The design of the “island-bridge” structure relies on a rigid backbone layer that restrains electrode deformation and stretchable, serpentine-shaped silver interconnection for a controlled strain distribution across the device. Compared to the common lactate BFC, the enhanced capacitance of the BSC is endowed to the synergistic effect of the CNT ink with the electrodeposited PPy conductive polymer on the anode and the high-surface-area porous Pt on the cathode. The resulting wearable bifunctional BSC supports high-power pulsed operation while maintaining stable cycling performance in human sweat-level lactate. High power of 0.343 mW cm^{-2} was achieved when the self-chargeable hybrid device is mounted on the arm of a human subject. When paired with voltage regulation components, commercial electronics, such as LEDs, can be successfully illuminated in pulsed mode by the designed BSC, suggesting its considerable potential as a power source for wearable electronics. As a wearable device with enzymatic electrodes, its stability may be affected by environmental factors, such as temperature, pH, salt ions, or surfactants, which will be assessed in the future. Future efforts will further optimize the operational conditions, cell performance, and electronics integration for advancing the capabilities and applications of this novel dual-functional self-charging device.

4. Experimental Section

Chemicals and Reagents: Polystyrene-block-polystyrene (SIS), toluene, NQ, glutaraldehyde bovine serum albumin (BSA), chitosan, Nafion (20%), L(+)-lactic acid, tetrahydrofuran (THF), terpineol, potassium phosphate dibasic (K_2HPO_4), and Ag flakes ($10 \mu\text{m}$) were purchased from Sigma Aldrich. Hydroxyl-functionalized multiwalled CNTs (OH-MWCNTs) (purity > 95%, diameter 10–20 nm, length 10–30 μm) were purchased from Cheap Tubes Inc., USA. LOx was purchased from Toyobo, Japan. Styrene ethylene butylene styrene copolymer was obtained from Kraton, TX, USA. PU (Tecoflex SG-80A) was obtained from Lubrizol Life Sciences, OH, USA. Ecoflex 00-30 was purchased from Smooth-On, Inc. PA, USA, and the Perme-roll Lite (L34R10) was obtained from Nitto Denko, Japan. Water-based PU resin Dispersoll U-42 and Bayhydur 302 crosslinker were purchased from Covestro. Ultra-pure deionized water ($18.2 \text{ m}\Omega$) was used for preparing all aqueous solutions.

Formulation of the Stretchable Ag ink and CNT Ink: The preparation of the stretchable Ag and CNT ink was similar to that reported in the previous work.^[21] The synthesis of Ag ink comprises the preparation of a polymeric resin consisting of 0.4 g mL^{-1} of SIS in toluene, then 0.7 g of the resin was mixed with 1.4 g of silver flakes in a dual asymmetric centrifugal mixer (Flacktek Speedmixer, DAC 150.1 KV-K, FlackTek, SC, USA) under a speed of 1800 rpm for 5 min. To enhance the mixing of the ink, Zirconia (YSZ) beads (3 mm, Inframat Advanced Materials, CT, USA) were also added. The CNT ink was synthesized by dispersing 100 mg OH-MWCNT in a solution containing 5 mL of THF and 0.5 mL of terpineol by probe sonication (FS-600 N, Ultrasonic processor, SX Ultrasonics, China) for 5 min. Thereafter, 100 mg of Tecoflex PU beads were added to the mixture and shaken for 12 h. The formulation of the PU interlayer was followed as previously reported,^[21] where 4 g of water-based PU resin was mixed with 250 mg of crosslinker before its deposition.

CNT Electrode Fabrication: A thin layer of Ecoflex was printed on the adhesive side of a Perme-Roll Lite film and cured at 65°C for 10 min to form the low elastic modulus substrate. The layers were printed using an MPM-SPM semi-automatic screen printer (Speedline Technologies, Franklin, MA, USA). A $100 \mu\text{m}$ -thick stainless-steel printing stencil was designed in AutoCAD (Autodesk, USA) and produced by laser-cut (Metal Etch Services, San Marcos, CA, USA). The printing process for the BSC was as follows: A rigid “island-like” structure layer was printed using the dielectric ink first onto the modified stretchable film and cured at 80°C for 15 min. Thereafter, to enhance the adhesion, the PU interlayer ink was printed on top of the dielectric layer and was cured at 80°C for 15 min. Then, the CNT ink was printed on top of the PU layer and cured at room temperature for 8 h followed by 30 min at 80°C . Finally, a stretchable conductive serpentine “bridge-like” structure layer was printed using the Ag-SIS ink and cured at 60°C for 15 min.

Electrodeposition of PPy and Pt: The electrodeposition of the PPy and porous Pt were performed in the three-electrode system, with Pt wire as the counter electrode and Ag/AgCl (in saturated KCl solution) as the reference electrode. The PPy deposition protocol followed previous work with minor changes.^[41] Shortly, a constant potential of 0.8 V versus Ag/AgCl was applied to the electrodes immersed into a solution containing 0.15 M pyrrole, 0.2 M K_2HPO_4 , and 5 mM $KClO_4$ for 20 s. A similar technique using commercial Pt electroplating solution was used to deposit the Pt cathode. A high potential of $E = -0.95$ V versus Ag/AgCl was set for 15 min to deposit the Pt with high porosity. After the electrodeposition, both electrodes were washed using deionized water four times and dried at room temperature.

Enzyme Modification of the Anode: The fabrication of the bioanode was performed by consecutively drop-casting solutions onto the CNT-based electrode surface. The sequence and the formulations of the drop-casting solutions for each electrode (0.16 cm^2) were as follows: First, a $5 \mu\text{L}$ 5 mg mL^{-1} of OH-MWCNTs dispersed in 0.2 M NQ in 9:1 vol/vol ethanol/acetone solution was cast. Subsequently, a $5 \mu\text{L}$ aliquot

of 40 mg mL⁻¹ LOx in 10 mg mL⁻¹ BSA and 5 μL of 1% glutaraldehyde solution were dropped cast and then covered with 5 μL of 1 wt% chitosan in 0.1 M acetic acid. Each of the above-mentioned steps was followed by a room temperature drying before adding the next layer. The chitosan layer was allowed to dry overnight.

Assembly of the BSC: A layer of Ecoflex was used to define the active area and insulate the exposed silver. A PVA-PBS electrolyte gel was prepared by dissolving 1 g of PVA in 5 g of deionized water and crosslinked with an equal weight of 3.3 M KOH solution in a desiccator until 80% weight was lost. After crosslinking, the hydrogel was repeatedly washed with 0.5 M PBS (pH of 7.4) to remove the excess KOH until reaching a neutral pH. The gel could be stored in PBS before use. The hydrogel was of high flexibility and conformity and was used in on-body experiments for sweat collection, establishing a secure interface between the skin and the electrodes (Figure S16, Supporting Information). Conductive stainless steel thin conductive threads (Adafruit, New York, USA) were used to connect the BSC to the output source using a silver conductive epoxy adhesive (8331, MG chemicals, Canada).

Electrochemical Measurements: Electrochemical studies of the BSC were carried out using μAutolab Type II. Oxygen reduction performance of the cathode was characterized using linear sweep voltammetry (LSV) at 5 mV s⁻¹ in 0.5 M PBS (pH 7.4). OCV of the BSCs was measured while quantified lactate solution was added to the 0.5 M PBS (pH 7.4). Polarization curves were obtained using LSV by scanning from OCV to 0 V at 5 mV s⁻¹. The geometrical area of each compartment, 0.64 cm², was used to calculate the areal power density. The stability of the BSC was analyzed by obtaining the polarization curve of the BSC every 2 h for up to 8 h in the presence of 10 mM lactate at room temperature. The ability of the BSC to deliver power in continuous mode was evaluated under galvanostatic discharge. The BSC was first immersed in 10 mM lactate for 3 min to reach stable OCV and then discharged from OCV to 0 V at 1 mA cm⁻². The capacitance of the BSC was characterized using CV and GCD techniques. For single electrode characterization, CV was performed in a three-electrode set-up. For the assembled cell characterization, CV was performed in a two-electrode set-up with the cathode as the working electrode and bioanode as the joint counter/reference electrode. CP was used to evaluate the performance of the BSC in the current pulse mode. For practical evaluation of the device performance, the minimum voltage value (V_{\min}) at the end of the pulse period was chosen. Power value was obtained by multiplying the current pulse and V_{\min} .

Characterization of the Materials and Electrodes: SEM (FEI Quanta FEG 250) was used to obtain morphological information of the printed electrodes. The element composition of the electrodes was characterized by energy dispersive X-ray mapping analysis.

Characterization of the Integrated Device: Mechanical tests of the BSC were performed using a motorized linear actuator coupled to a programmable controller (A-LST0250A-E01 Stepper Motor and Controller, Zaber Technologies, BC, Canada). The BSC was stretched repeatedly by 20% at a speed of 0.1 cm s⁻¹ from 0% to 20% reversibly. The resistance change was recorded using a digital multimeter (34411A, Agilent Technologies, CA, USA). The on-body test was performed by attaching the BSC device facing down to the skin of the arm. A thin film of Perme-Roll Lite was used to hold and insulate the device onto the skin. Stainless steel thin conductive threads were used to connect the device into output, and silver conductive epoxy was used in the interconnections. All the on-body tests were carried out with consent from the subject volunteers, approved by the Human Research Protections Program at the University of California, San Diego, and in strict compliance with the guidelines of Institutional Review Boards (IRB). The LED pulsed illumination test was conducted by connecting two BSC patches in parallel and adding the PBS solution with respective lactate concentrations onto the patch. The patch was connected to a BQ25504 Power Management chip (Texas Instrument, TX, USA) with a complementary circuit, with the output connected to a yellow LED (Sparkfun, CO, USA).

The connection was controlled manually. A digital multimeter and a potentiostat were used to simultaneously monitor the current and voltage through/across the LED.

Supporting Information

Supporting Information is available from the Wiley Online Library or from the author.

Acknowledgements

J.L., L.Y., X.C., and I.J. contributed equally to this work. The authors acknowledge support from the Pack Ambition International Région Auvergne-Rhône-Alpes n° 20 006921 01-91830. X.C. is grateful for a Université Grenoble Alpes Ph.D. scholarship and IDEX for funding X.C.'s travel grant. I.J. acknowledges support from Thai Development and Promotion of Science and Technology Talents Project (DPST). C.A.S. acknowledges support from UC MEXUS-CONACYT fellowship.

Conflict of Interest

The authors declare no conflict of interest.

Data Availability Statement

The data that support the findings of this study are available from the corresponding author upon reasonable request.

Keywords

biosupercapacitors, energy harvesting, self-charging biosupercapacitors, stretchable electronics, wearable electronics

Received: March 25, 2021

Revised: June 13, 2021

Published online:

- [1] J. Wang, M.-F. Lin, S. Park, P. S. Lee, *Mater. Today* **2018**, *21*, 508.
- [2] L. Yin, J. Lv, J. Wang, *Adv. Mater. Technol.* **2020**, *5*, 2000694.
- [3] J. Kim, I. Jeerapan, J. R. Sempionatto, A. Barfidokht, R. K. Mishra, A. S. Campbell, L. J. Hubble, J. Wang, *Acc. Chem. Res.* **2018**, *51*, 2820.
- [4] C. Wang, X. Li, H. Hu, L. Zhang, Z. Huang, M. Lin, Z. Zhang, Z. Yin, B. Huang, H. Gong, S. Bhaskaran, Y. Gu, M. Makihata, Y. Guo, Y. Lei, Y. Chen, C. Wang, Y. Li, T. Zhang, Z. Chen, A. P. Pisano, L. Zhang, Q. Zhou, S. Xu, *Nat. Biomed. Eng.* **2018**, *2*, 687.
- [5] C. Yan, J. Wang, W. Kang, M. Cui, X. Wang, C. Y. Foo, K. J. Chee, P. S. Lee, *Adv. Mater.* **2014**, *26*, 2022.
- [6] J. R. Sempionatto, M. Lin, L. Yin, E. De la Paz, K. Pei, T. Sosa-ard, A. N. de Loyola Silva, A. A. Khorshed, F. Zhang, N. Tostado, S. Xu, J. Wang, *Nat. Biomed. Eng.* **2021**, <https://doi.org/10.1038/s41551-021-00685-1>.
- [7] D.-H. Kim, N. Lu, R. Ma, Y.-S. Kim, R.-H. Kim, S. Wang, J. Wu, S. M. Won, H. Tao, A. Islam, K. J. Yu, T.-i. Kim, R. Chowdhury, M. Ying, L. Xu, M. Li, H.-J. Chung, H. Keum, M. McCormick, P. Liu,

- Y.-W. Zhang, F. G. Omenetto, Y. Huang, T. Coleman, J. A. Rogers, *Science* **2011**, 333, 838.
- [8] T. Sekitani, H. Nakajima, H. Maeda, T. Fukushima, T. Aida, K. Hata, T. Someya, *Nat. Mater.* **2009**, 8, 494.
- [9] W. Gao, S. Emaminejad, H. Y. Y. Nyein, S. Challa, K. Chen, A. Peck, H. M. Fahad, H. Ota, H. Shiraki, D. Kiriya, D.-H. Lien, G. A. Brooks, R. W. Davis, A. Javey, *Nature* **2016**, 529, 509.
- [10] S. Gong, W. Cheng, *Adv. Energy Mater.* **2017**, 7, 1700648.
- [11] X. Pu, W. Hu, Z. L. Wang, *Small* **2018**, 14, 1702817.
- [12] X. Gong, Q. Yang, C. Zhi, P. S. Lee, *Adv. Energy Mater.* **2021**, 11, 2003308.
- [13] L. Yin, J. Scharf, J. Ma, J.-M. Doux, C. Redquest, V. L. Le, Y. Yin, J. Ortega, X. Wei, J. Wang, Y. S. Meng, *Joule* **2021**, 5, 228.
- [14] A. J. Bandodkar, J. Wang, *Electroanalysis* **2016**, 28, 1188.
- [15] L. Ma, Y. Zhao, X. Ji, J. Zeng, Q. Yang, Y. Guo, Z. Huang, X. Li, J. Yu, C. Zhi, *Adv. Energy Mater.* **2019**, 9, 1900509.
- [16] A. J. Bandodkar, J.-M. You, N.-H. Kim, Y. Gu, R. Kumar, A. M. V. Mohan, J. Kurniawan, S. Imani, T. Nakagawa, B. Parish, M. Parthasarathy, P. P. Mercier, S. Xu, J. Wang, *Energy Environ. Sci.* **2017**, 10, 1581.
- [17] I. Jeerapan, J. R. Sempionatto, A. Pavinatto, J.-M. You, J. Wang, *J. Mater. Chem. A* **2016**, 4, 18342.
- [18] A. J. Bandodkar, *J. Electrochem. Soc.* **2016**, 164, H3007.
- [19] S. Yin, X. Liu, T. Kaji, Y. Nishina, T. Miyake, *Biosens. Bioelectron.* **2021**, 179, 113107.
- [20] X. Chen, L. Yin, J. Lv, A. J. Gross, M. Le, N. G. Gutierrez, Y. Li, I. Jeerapan, F. Giroud, A. Berezovska, R. K. O'Reilly, S. Xu, S. Cosnier, J. Wang, *Adv. Funct. Mater.* **2019**, 29, 1905785.
- [21] J. Lv, I. Jeerapan, F. Tehrani, L. Yin, C. A. Silva-Lopez, J.-H. Jang, D. Joshua, R. Shah, Y. Liang, L. Xie, F. Soto, C. Chen, E. Karshalev, C. Kong, Z. Yang, J. Wang, *Energy Environ. Sci.* **2018**, 11, 3431.
- [22] L. Yin, K. N. Kim, J. Lv, F. Tehrani, M. Lin, Z. Lin, J.-M. Moon, J. Ma, J. Yu, S. Xu, J. Wang, *Nat. Commun.* **2021**, 12, 1542.
- [23] W. Zuo, R. Li, C. Zhou, Y. Li, J. Xia, J. Liu, *Adv. Sci.* **2017**, 4, 1600539.
- [24] H. C. Chen, Y. Qin, H. Cao, X. Song, C. Huang, H. Feng, X. S. Zhao, *Energy Storage Mater.* **2019**, 17, 194.
- [25] D. Pankratov, P. Falkman, Z. Blum, S. Shleev, *Energy Environ. Sci.* **2014**, 7, 989.
- [26] P. Bollella, Z. Boeva, R.-M. Latonen, K. Kano, L. Gorton, J. Bobacka, *Biosens. Bioelectron.* **2021**, 176, 112909.
- [27] T. Bobrowski, E. González Arribas, R. Ludwig, M. D. Toscano, S. Shleev, W. Schuhmann, *Biosens. Bioelectron.* **2018**, 101, 84.
- [28] Y. Jang, T. Park, E. Kim, J. W. Park, D. Y. Lee, S. J. Kim, *Angew. Chem., Int. Ed.* **2021**, 60, 10563.
- [29] S. Shleev, E. González-Arribas, M. Falk, *Curr. Opin. Electrochem.* **2017**, 5, 226.
- [30] K. L. Knoche, D. P. Hickey, R. D. Milton, C. L. Curchoe, S. D. Minteer, *ACS Energy Lett.* **2016**, 1, 380.
- [31] D. Pankratov, Z. Blum, D. B. Suyatin, V. O. Popov, S. Shleev, *ChemElectroChem* **2014**, 1, 343.
- [32] M. Zhu, Y. Huang, Y. Huang, H. Li, Z. Wang, Z. Pei, Q. Xue, H. Geng, C. Zhi, *Adv. Mater.* **2017**, 29, 1605137.
- [33] L. Yin, J. K. Seo, J. Kurniawan, R. Kumar, J. Lv, L. Xie, X. Liu, S. Xu, Y. S. Meng, J. Wang, *Small* **2018**, 14, 1800938.
- [34] R. Wannapob, M. Yu. Vagin, I. Jeerapan, W. C. Mak, *Langmuir* **2015**, 31, 11904.
- [35] M. Yu. Vagin, I. Jeerapan, R. Wannapob, P. Thavarungkul, P. Kanatharana, N. Anwar, T. McCormac, M. Eriksson, A. P. F. Turner, E. W. H. Jager, W. C. Mak, *Electrochim. Acta* **2016**, 190, 495.
- [36] L. Yin, R. Kumar, A. Karajic, L. Xie, J. You, D. Joshua, C. S. Lopez, J. Miller, J. Wang, *Adv. Mater. Technol.* **2018**, 3, 1800013.
- [37] X. Zhang, Bai, *Langmuir* **2003**, 19, 10703.
- [38] F. Conzuelo, N. Marković, A. Ruff, W. Schuhmann, *Angew. Chem., Int. Ed.* **2018**, 57, 13681.
- [39] A. J. Bandodkar, I. Jeerapan, J.-M. You, R. Nuñez-Flores, J. Wang, *Nano Lett.* **2016**, 16, 721.
- [40] P. Mercier, J. Wang, *IEEE Spectrum* **2020**, 57, 28.
- [41] A. Fakhry, H. Cachet, C. Debiemme-Chouvy, *Electrochim. Acta* **2015**, 179, 297.